Izvestiya, Atmospheric and Oceanic Physics

Vol. 28, No. 3, 1992
UDC 551.521.32:551.510.53

The Spectral Structure of the Nonequilibrium Outgoing Limb Radiance in the 15 μm CO_2 Absorption Band

V. S. KOSTSOV, V. V. ROZANOV, YU. M. TIMOFEYEV, K. H. GRASSL AND A. A. KUTEPOV

St. Petersburg State University
Max Planck Institute of Meterology

The formational features of outgoing limb radiance in the spectral line profiles of the 15 μm CO_2 absorption band are investigated under nonlocal thermodynamic equilibrium conditions for slant paths with tangent heights of 50-110 km. High-resolution spectra are calculated for the outgoing nonequilibrium limb radiance, and their variations attributable to variations in kinetic and vibrational temperatures are analyzed. The possibility of recovering information on the vertical distributions of the vibrational temperatures from radiation measurements is demonstrated, and an estimate of the optimal spectral resolution for solving this problem is obtained.

1. Spectral and angular measurements of outgoing atmospheric limb radiance are widely used today for remote temperature measurements and determination of the composition of the atmosphere [1-3]. In the case of a slant (at the planetary horizon) measurement profile, the maximum altitude of passive measurements with traditional techniques is determined largely by the violation of local thermodynamic equilibrium (LTE). Modern requirements for obtaining global information on the temperature structure and composition of the upper atmospheric layers have stimulated an analysis of the effect of disruptions in local thermodynamic equilibrium on the accuracy of passive sounding and the development of a number of new methods of interpreting measurements under non-LTE conditions [4-7]. In [5, 6] the possibilities of solving a number of inverse problems in the 15 μm CO_2 band (restoration of the kinetic temperature profile, the radiation survival probability, etc.), are examined by means of measurements of moderate spectral resolution. The rather limited information capabilities of such measurements in the actual formulation of the problem are demonstrated.

The development of the experimental technique has made it possible in recent years to fabricate equipment for high-precision, high-resolution ($\Delta\nu$ = 0.01-0.1 cm^{-1}) measurements of atmospheric limb radiance [8-10]. This makes an analysis of the formational features of nonequilibrium limb radiance under non-LTE conditions an important problem as a first step towards developing new approaches to interpreting high resolution measurements for purposes of obtaining information on the parameters of the physical state of the upper atmospheric layers. This paper analyzes calculation results of monochromatic outgoing limb radiance in the spectral line profiles and the high-resolution spectra in the Q branches of the 15 μm CO_2 band. We also analyze the structure of the spectrum of limb radiance variations attributable to temperature variations, which permits a simple characterization of the possibilities for solving the inverse problem of thermal sounding of the upper atmospheric layers (15-110 km) were deviation from LTE conditions is most significant.

2. The solution of the transport equation for monochromatic outgoing limb radiance on slant paths can be written as

$$I_\nu(h_0) = \int_0^{s_0} \alpha_\nu(s) J_\nu(s) \exp\left[-\int_0^s \alpha_\nu(s')ds'\right] ds, \qquad (1)$$

where $I_\nu(h_0)$ is the monochromatic limb radiance intensity at frequency ν for a tangent height h_0; s is the coordinate along the optical path; $s = 0$ and s_0 are the boundaries of the optically active atmosphere; and α_ν and J_ν represent the bulk absorption coefficient and the source function at frequency ν for which the following expressions are valid

$$\alpha_\nu = \Sigma \sigma_{\nu,v'j'vj}, \quad J_\nu = \frac{\Sigma \sigma_{\nu,v'j'vj} S_{v'j'vj}}{\Sigma \sigma_{\nu,v'j'vj}}, \qquad (2)$$

where $\alpha_{\nu,v'j'vj}$ and $S_{v'j'vj}$ is the absorption coefficient and source function at the spectral line corresponding to the $v'j' \to vj$ transition (v and j are the vibrational and rotational quantum number, respectively); summation in the general case is over the spectral lines of all gases and their isotopes.

0001-4338/93/2803-0008$18.00/1

In the case of non-LTE conditions, a calculation of $\sigma_{\nu,v'j'vj}$ and $S_{v'j'vj}$ requires knowledge of the nonequilibrium populations of the molecular vibrational-rotational states, which can be expressed through the vibrational temperatures of the corresponding states. We then have for the source function and the absorption coefficient at the spectral line:

$$S_{v'j'vj} = \frac{2h\nu^3_{v'j'vj}}{c^2}\left[\exp\left(\frac{E_{v'}}{kT_{v'}} - \frac{E_v}{kT_v} + \frac{E_{j'}-E_j}{kT}\right) - 1\right]^{-1}, \quad (3)$$

$$\sigma_{v'j'vj} = S_0 \frac{W(T, T_{v'}, T_v)}{w(T^*)} n_0 f_k(\nu, \nu_{v'j'vj}), \quad (4)$$

where h and k are the Planck and Boltzmann constant; c is the speed of light; $\nu_{v'j'vj}$ is the frequency of the $v'j' \to vj$ transition; $E_{v'}$, E_v, $E_{j'}$ and E_j are the energies of the corresponding vibrational and rotational states; T is the kinetic temperature; $T_{v'}$ and T_v are the vibrational temperatures of the corresponding states; n_0 is the molecular concentration; S_0 is the line intensity per molecule at a standard temperature T^*; and f_k is a function describing the spectral line profile. The functions $w(T^*)$ and $W(T, T_{v'}, T_v)$ are described by means of the relations

$$w(T^*) = \frac{1}{(T^*)^m}\exp\left[\frac{E_{vj}}{kT^*}\right]\left[1 - \exp\left(\frac{h\nu_{v'j'vj}}{kT^*}\right)\right], \quad (5)$$

$$W(T, T_{v'}, T_v) = \frac{1}{T^m}\exp\left[-\frac{E_v}{kT_v} - \frac{E_j}{kT}\right]\left[1 - \exp\left(-\frac{E_{v'}}{kT_{v'}} + \frac{E_v}{kT_v} - \frac{E_{j'}-E_j}{kT}\right)\right]. \quad (6)$$

Here m is the exponent in the approximation of the temperature dependence of the statistical sum, $E_{vj} = E_v + E_j$. The parameters of the fine structure ($\nu_{v'j'vj}$, S_0, E_{vj}, etc.) for calculating the outgoing limb radiance based on these equations were borrowed from the HITRAN spectroscopic data base [11]; the Voight profile was used for f_k.

Under LTE conditions $T_{v'} = T_v = T$ (T is the kinetic temperature) and Eq. (3) becomes the well-known Planck function of black body radiation, while Eq. (4) becomes the standard expression for the absorption coefficient. Note that it was assumed that LTE held over the rotational states in deriving Eqs. (3) and (4), which is valid for CO_2 molecules through altitudes of $\sim$ 150 km [12].

The nonequilibrium populations of the vibrational levels of the CO_2 molecules (the vibrational temperatures) were calculated by the method described in [12] for the kinetic temperature profile of the U.S. standard (1976) model. The CO_2 profile was borrowed from [13]. In this case, deviations from LTE were taken into account only for the seven lower vibrational states whose transitions play a fundamental role in producing the outgoing limb radiance in the 15 μm band on slant paths for $h_0 \geqslant 50$ km. These states are $01^10.02^00.02^2$ $0.10^00.03^10.03^30$ and 11^10. Henceforth, these will be denoted by ordinal numbers from 1 through 7 (the unexcited ground state will be represented by zero); we use the designations T_1, T_2, ..., T_7 for the corresponding vibrational temperatures. Deviations from LTE conditions begin to be manifested at altitudes of 70-80 km, where they are still insignificant. These deviations become significant above 90 km where the "nonequilibrium" atmosphere becomes significantly "colder" than the "equilibrium" atmosphere for this model. Thus, T_ν of the 01^10 (T_1) vibrational level at an altitude 90 km is 11 K below the kinetic temperature and at an altitude of 115 km is 125 K below this temperature. Another feature of the vibrational temperature distributions is the near constancy of T_ν over the mesopause at altitudes between 95 and 105 km. The range of vibrational temperatures is substantially smaller overall compared to the kinetic temperature: from 160 to 210 K.

It was necessary to account for the contribution of lines in the range $\nu \pm 0.5$ cm^{-1} in calculating α_ν and J_ν to achieve accuracy in the calculations of the 0.2 K outgoing limb radiance in terms of the brightness temperature. Specifically, this suggests that the isolated line approximation which is widely used in various calculations (for example, [12]) may produce significant errors in calculating the outgoing limb radiance on slant paths.

3. The primary factors responsible for the features of the spectral and altitude structures of the nonequilibrium outgoing limb radiance on slant paths are as follows:

(a) the significant variability of the absorption coefficient $\sigma_\nu(s)$ (and, consequently, the optical thicknesses $\tau_\nu(s)$) at the spectral line profile;

(b) the vertical course of the kinetic and vibrational temperatures of the various CO_2 molecular states;

(c) the varying functional dependence of σ_ν on pressure on the wings and at the center of the spectral lines;

(d) the decrease in CO_2 concentration with altitude.

Figure 1 provides the relation $\tau_\nu(0, s)$ along the path of the outgoing limb radiance ($s = 0$ corresponds to the upper atmospheric boundary nearest the instrument) for five frequencies in the strong line profile belonging to the Q branch of the fundamental $1 \to 0$ transition ($\nu_0 = 667.9034$ cm^{-1}, $S_0 = 0.2594 \cdot 10^{-18}$ cm^{-1}·mod^{-1}·cm^2) for $h_0 = 70$ km. It follows from Fig. 1 that $\tau_\nu(0, s)$ varies along the path and varies of 12 orders of magnitude within the range $|\nu - \nu_0| = 0.0074$ cm^{-1}. If the optical

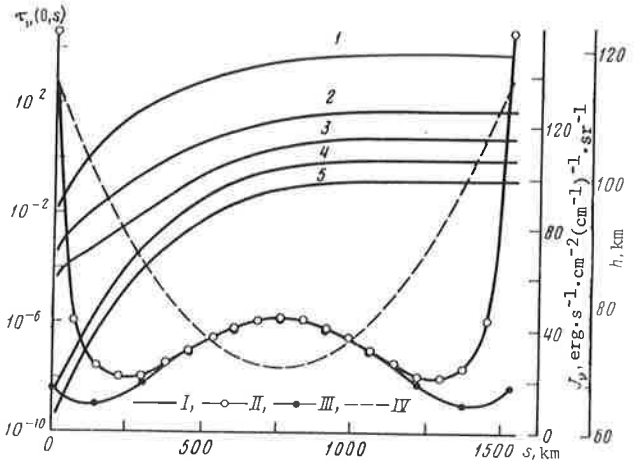

Fig. 1. Characteristics of limb radiance transport on a slant path for a tangent height h_0 = 70 km for five different frequencies at the line profile of the fundamental transition: ν_0 = 667.9034 cm^{-1}: 1) 667.9034; 2) 667.9048; 3) 667.9052; 4) 667.9066; 5) 667.9108 cm^{-1}; I--optical thickness; II--source function (LTE); III--source function (non-LTE); IV--height h as a function of the path coordinate.

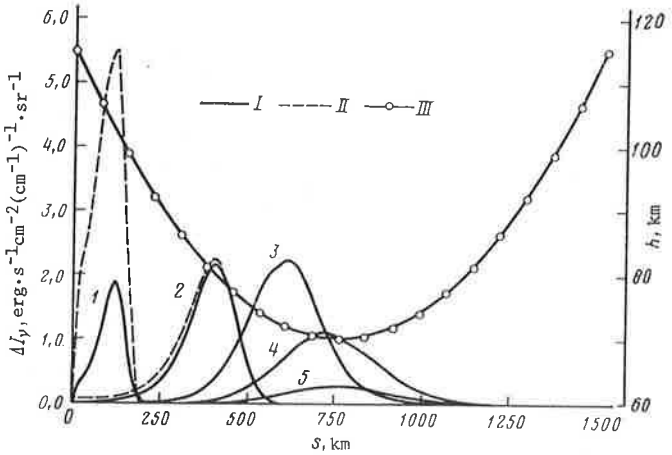

Fig. 2. Contributions of finite segments of the optical path (tangent height h_0 = 70 km) to limb radiance for a number of frequencies in the line profile of the fundamental transition ν_0 = 667.9034 cm^{-1} (see the legend to Fig. 1). I--on-LTE; II--LTE; III--altitude as a function of the path coordinate.

thicknesses reach $\sim 10^4$ at the center of the line, at the wing they are $\sim$ 0.3. Figure 1 also shows the spatial course of the source functions for equilibrium and nonequilibrium conditions reflecting the differences of the kinetic and vibrational temperatures. There are significant deviations of the source functions from their equilibrium values at the initial and final $\sim$ 350-km path sections ($z \geqslant 85$ km); these deviations are quite significant at high altitudes and reach a maximum of $\sim$100 erg·s^{-1}·cm^{-2}·(cm^{-1})$^{-1}$·sr^{-1} or more. (Note that the changes in $\tau_\nu(0,s)$, attributable to the nonuniformity are not significant and are not noticeable on the scale selected for (Fig. 1.)

The effect of the various functional dependences of the absorption coefficient on pressure

Table 1

Distribution of the Radiating Layers in the Contour of the Line

$\nu_0 = 667.9034\ cm^{-1}$, $h_0 = 70$ km

	Tangency $\nu - \nu_0$, cm^{-1}				
	0	0,0014	0,0018	0,0032	0,0074
Distance from the point of tangency along the path, km	630	340	140	50	0
Altitude, km	~102	~80	~71	~70	~70

p is revealed in Fig. 1 by the more rapid growth of $\tau_\nu(0, s)$ for the frequencies along the line wing, since $\sigma_\nu \sim p$, for these frequencies at the same time that for $\nu = \nu_0$ there is no such relation for the Doppler line profile, while $\sigma_\nu \sim p^{-1}$ for the Lorentz line profile.

Figure 2 provides a convenient representation of the formation of outgoing limb radiance along the path ($h_0 = 70$ km) for different frequencies in the same spectral line profile where the contributions (ΔI_ν) to the outgoing limb radiance from the 15-km path sections are shown. At the center of the line, radiation is formed in the outer layers of the atmosphere near the instrument due to the high optical thicknesses (see Fig. 1) at altitudes of 100-110 km and at distances of ~ 6 km from the tangent point ($s = 750$ km). In this case $\tau_\nu(0, s)$ decreases in the transition from the line center to the wing and the limb radiance layers approach the tangent point, while shifting to lower levels. The quantitative characteristics of the radiating layers for the different frequencies in the line profile are shown in Table 1. It is also clear from Table 2 that for this tangent height $h_0 = 70$ km the effect of nonequilibrium will be significant only near the line center, and the weak effect of nonequilibrium on the optical density will cause the limb radiance formation regions to be roughly identical under both LTE and non-LTE conditions.

The features of outgoing limb radiance formation on the slant paths suggest that high spectral resolution measurements of I_ν will contain certain information on the state of the atmosphere along the limb radiance propagation path with difference values of h_0. Therefore, this feature can be used to develop remote methods of sounding a spherically inhomogeneous atmosphere in which, for example, the temperature is a function not only of altitude but also of latitude. Note that all traditional oblique-incidence sounding methods have been formulated for a spherically homogeneous atmosphere [1, 3] and that a significant drawback of these methods is the significant horizontal averaging of the desired atmospheric parameters. (The idea of the possibility for two-dimensional thermal sounding based on 15 μm band measurements was first suggested in [14]). Note that these features of outgoing limb radiance formation have been observed in a narrow spectral interval near the line center ($\Delta\nu \sim 0.01\ cm^{-1}$), which imposes stringent requirements on the spectral resolution of the instruments for implementation of two-dimensional sounding.

Figure 3 shows the calculation results of the outgoing limb radiance (in terms of the radiance temperature T_r) for different tangential altitudes for both equilibrium and nonequilibrium (LTE and non-LTE) conditions in this line profile. It follows from the figure that different types of spectral behavior of $T_r(\nu)$ (and, consequently, the radiance) are observed depending on h_0:

(a) the limb radiance line (for example, $h_0 = 90$, 110 (LTE) and $h_0 = 110$ km (non-LTE));

(b) the absorption line ($h_0 = 50$ km (non-LTE));

(c) complex behavior of $T_r(\nu)$ characterized by peaks away from the line center ($h_0 = 50$ and 70 km (LTE), $h_0 = 70$, 90 km (non-LTE)).

Such a varied behavior of $T_r(\nu)$ is due to the features of outgoing limb radiance formation on the slant paths. Thus, for example, the limb radiance at the line center for $h_0 = 70$ km in a nonequilibrium atmosphere forms along the outer edge of the route at altitudes of $z = 100$-110 km as a result of the high optical density; here, the vibrational temperature profile of the 1 $T_1(z)$ state is near-isothermic, and $T_1 \sim 167$ K. Therefore, T_r at the line center will have nearly the same value. The radiating layers shift towards lower and warmer atmospheric regions away from the line center and with decreasing optical thickness, and peaks of $T_r \approx 210$ K are observed for $|\nu - \nu_0| \sim 0.002\ cm^{-1}$. The atmosphere becomes semitransparent at the line wings and a monotonic decrease in T_r attributable to the decreasing irradiance is observed.

The effect of a nonequilibrium atmosphere is more strongly manifested at the line center where

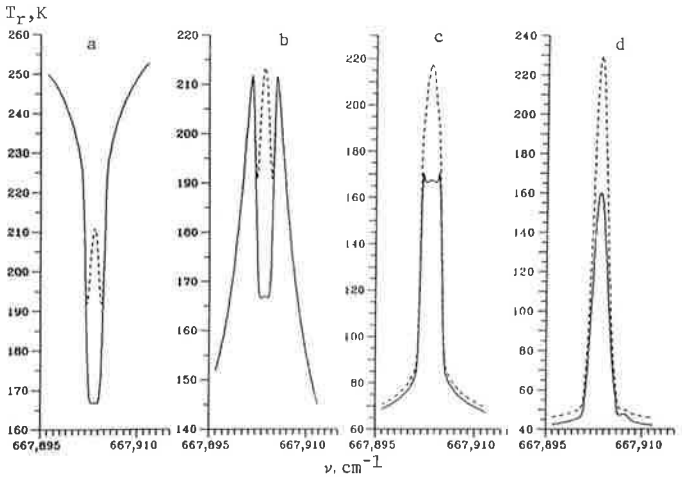

Fig. 3. Outgoing limb radiance on slant paths (in terms of the radiance temperature) in the spectral line profile of the fundamental transition ν_0 = 667.9034 cm^{-1} for h_0 = = 50 (a), 70 (b), 90 (c), and 100 km (d). The solid lines correspond to non-LTE conditions, and the dashed line corresponds to LTE conditions.

the differences in T_r for LTE and non-LTE conditions are ∿50 K for h_0 = 50-90 km, and increase to 70 K for h_0 = 110 km. The loss of LTE begins to be manifested at values of T_r along the line wings for $H_0 \geqslant 90$ km and serves to reduce T_r by 2-5 K. The nonequilibrium effects at the center of the line are already manifested at a tangent height of h_0 = 50 km, which is substantially below the level of loss of LTE for the 1 vibrational state (∿ 70 km). (Such an effect was identified in [15] for the 4.7 μm CO_2 lines.) It should be emphasized that the spectral structure of the outgoing nonequilibrium limb radiance is fundamentally different from the structure of equilibrium limb radiance, which reflects differences in the kinetic and vibrational temperature profiles for a number of values of h_0 (50, 70, and 90 km).

4. We now analyze the spectra of outgoing limb radiance for finite spectral resolution. Let us consider the range 666-671 cm^{-1}, which is of primary interest from the viewpoint of thermal sounding of the upper atmospheric layers, since these layers contain the most intensive lines in the 15 μm CO_2 band.

Figure 2 shows the spectra of the outgoing limb radiance for tangent heights h_0 = 70, 85, and 100 km at a resolution of $\Delta\nu$ = 0.1 cm^{-1} for LTE and non-LTE cases. The spectra clearly reveal three peaks corresponding to the most intensive lines of the Q branches of the 1→0, 3→0, and 6→3 transitions centered at frequencies 667.5, 667.8 and 688.2 cm^{-1}, respectively. The equilibrium and nonequilibrium limb radiance spectra are similar in form and transform identically with changing tangent height. The radiation corresponding to non-LTE conditions is lower for all tangent heights compared to the equilibrium value, which is due to the lower vibrational temperatures compared to the kinetic temperature. It is clearly evident that the differences between the equilibrium and nonequilibrium limb radiance $\delta I_{\text{non-LTE}}$ (the curves with the asterisks) are weakly dependent on the tangent height and in the range containing the Q branch lines equal 1-2 erg·s^{-1}·cm^{-2}·(cm^{-1})$^{-1}$·sr^{-1}. The maximum values of $\delta I_{\text{non-LTE}}$ occur at the Q branch of the fundamental 1 → 0 transition, where the waveform of the $\delta I_{\text{non-LTE}}$ spectrum, like the values themselves, remains virtually unchanged with tangent height. The constant values of $\delta I_{\text{non-LTE}}$ can be attributed to the fact that limb radiance for different values of h_0 is formed largly along the outer section of the optical path, i.e., in layers z = 90-110 km, where LTE breaks down in regions characterized by strong absorption. Consequently, even for slant paths with tangent heights that are lower than the level of LTE breakdown in the atmosphere, the intensity of the outgoing radiation will contain a nonequilibrium component of the same order of magnitude as the component noted above.

Variations in the outgoing limb radiance attributable to variations in the temperature profile δI_T were also calculated for LTE and non-LTE conditions. Note that temperature variations at all altitude levels were assumed to be equal to

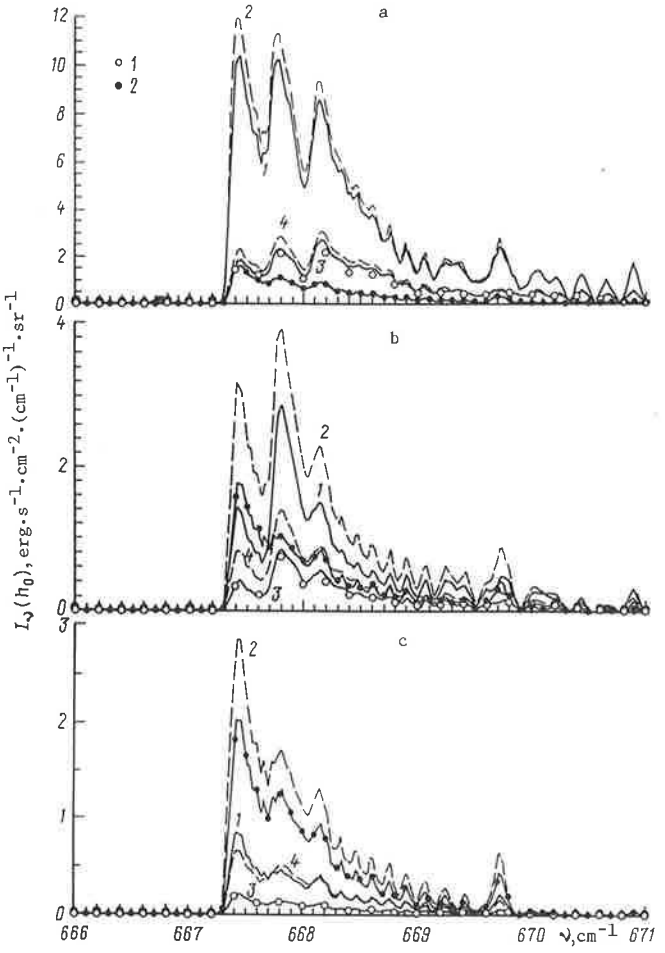

Fig. 4. Outgoing limb radiance in the range of the most intensive transitions of the 50 μm CO_2 band for slant paths with different tangent heights: h_0 = 70 (a), 85 (b), and 100 km (c). The spectral resolution $\Delta\nu$ = 0.1 cm^{-1}. 1, 3) the limb radiance and its variation δI_T under non-LTE conditions; 2, 4) the same LTE conditions. The solid circles represent the difference between the equilibrium and nonequilibrium values $I_{\text{LTE}} - I_{\text{non-LTE}}$; the open circles represent the values of δI_T calculated in a linear approximation.

10 K. In this case, variations in the vibrational temperatures obtained by solving stationary equations ranged from 10 K at 70-80 km to 5-6 K at ∿110 km. As we see from the figure, the spectral behavior of δI_T is the same as that of the limb radiance itself. With this spectral resolution, near the peaks δI_T will account for 10-20% of the intensity values. The open circles in the figure represent the values of δI_T calculated in a linear approximation. As we see, for the given temperature variations of 10 K the linear approximation is accurate to better than ∿15% in a range of tangent heights of 70-110 km, which makes it possible to analyze the sum spectral components δI_T attributable to the contribution of the kinetic temperature $\delta I[\delta T(z)]$ and the vibrational temperature $\delta I[\delta T_i(z)]$ (i = 1, ..., 7) individually (the so-called individual variations):

$$\delta I_T \approx \delta I[\delta T(z)] + \sum_{i=1}^{7} \delta I[\delta T_i(z)]. \qquad (7)$$

The values of $\delta I[\delta T(z)]$ and $\delta I[\delta T_i(z)]$ calculated in a linear approximation are shown in Fig. 5 for two tangent heights h_0 = 70 and 85 km (the left and right scales, respectively). The greatest absolute variations in limb radiance observed in this spectral domain are attributable to temperature

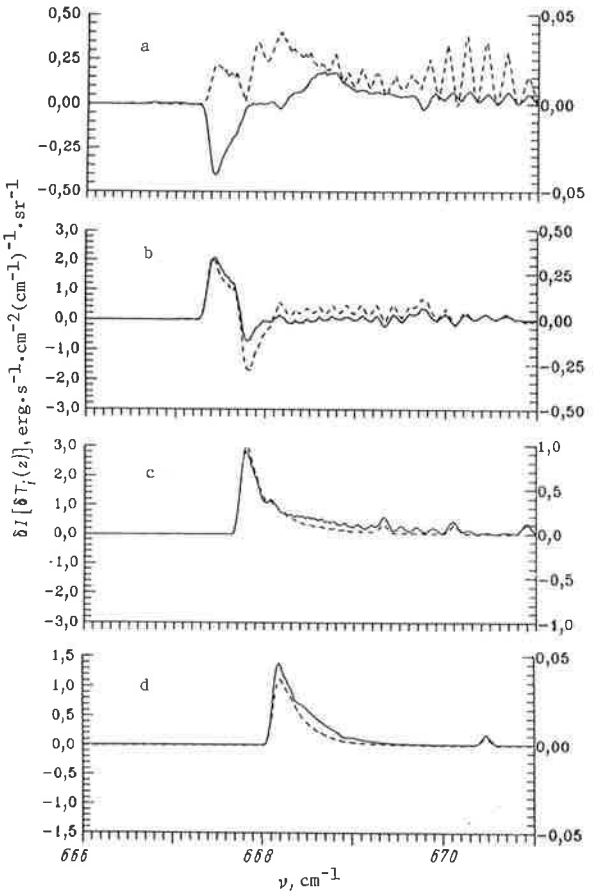

Fig. 5. Individual variations in the limb radiance for h_0 = 70 km (left scales, solid lines) and 85 km (right scales, dashed line): $\delta I_{\Delta\nu}[\delta T(z)]$ (a); $\delta I_{\Delta\nu}[\delta T_1(z)]$ (b); $\delta I_{\Delta\nu}[\delta T_3(z)]$ (c); $\delta I_{\Delta\nu}[\delta T_5(z)]$ (d). The spectral resolution $\Delta\nu$ = = 0.1 cm^{-1}.

variations T, T_1, T_3, and T_6. Variations $\delta I[\delta T_{2,4,5,7}(z)]$ are within an order of magnitude or lower. The data shown in Fig. 5 conveniently demonstrate the spectral "separation of variables" at a spectral resolution $\Delta\nu$ = 0.1 cm^{-1}. It is quite obvious that measurements at an average spectral resolution (for example $\Delta\nu$ = 1-5 cm^{-1}) do not have this capability.

It should also be noted that individual variations may be of different sign and also may reverse sign with changing h_0, which reflects the effect of multiple factors. With increasing tangent, height $\delta I[\delta T_i(z)]$ drop off significantly, which is consistent with the data shown in Fig. 5. Note also the small values of δI with changing kinetic temperature, which is due to the small differences in the rotational energies of the transitions producing the Q branches.

The numerical values of variations in the outgoing limb radiance for a single frequency near the other Q branch in the 15 μm CO_2 band for different values of h_0 are listed in Table 2. The table also shows variations with the most influential temperatures: T, T_1, T_2, T_3, and T_5. Variations of $\delta I_{\Delta\nu}[\delta T_i(z)]$ for other T_i (T_4, T_6, and T_7) are either equal to zero or are negligible.

As noted above, all variations decrease with increasing h_0, have different signs, and may reverse sign as h_0 changes. The maximum variations (and, consequently, optimal potential determination capabilities) are observed for T_1, T_2, T_3 and T_5. As in the range 666-671 cm^{-1}, variations of $\delta I_{\Delta\nu}[\delta T(z)]$ are not significant in absolute terms for h_0 > 80 km.

To analyze the possibility of obtaining information on the actual thermal state of the atmosphere, we introduce the signal-to-noise ratio S/N where S represents the absolute variations in outgoing limb radiance and N represents the mean square error of measurements produced by the specific satellite instruments. For example, for the MIPAS interferometer for a resolution of $\Delta\nu$ = 0.05, 0.1, 0.2 cm^{-1} the value of N will adopt values of 0.4, 0.2, and 0.1. erg·s^{-1}·cm^{-2}·(cm^{-1})$^{-1}$·sr^{-1}, respectively. Figure 6 shows the spectra of variations in the outgoing limb radiance δI_T for different values of $\Delta\nu$ at a tangent height h_0 = 90 km. An analysis of the effect of spectral resolution on variations makes it possible to determine the "optimal" $\Delta\nu$ which realizes, on the one hand, the maximum S/N radio and, on the other, makes it possible to separate the contributions of variations $\delta I_{\Delta\nu}[\delta T_i(z)]$ attributable to different vibrational transitions. We estimate that such an "optimal" resolution is ∿0.2 cm^{-1}. At this resolution and at the noise level corresponding to the MIPAS interferometer (0.1 erg·s^{-1}·cm^{-2}·(cm^{-1})$^{-1}$·sr^{-1}), the S/N ratios for h_0 = 90 km are 2.5-4.5 for different frequencies in the range 661-671 cm^{-1} (see Fig. 6) and are significantly higher than for $\Delta\nu$ = = 0.05 cm^{-1}. The S/N ratio decreases with increasing tangent height, although, as demonstrated by the calculations, for h_0 = 100 km and, for example, at $\Delta\nu$ = 0.2 cm^{-1}, the S/N ratio exceeds unity near the most intensive lines at the same time that for $\Delta\nu$ < 0.2 cm^{-1}, S/N < 1. The data shown in Fig. 6 also suggest that although a further degradation in the spectral resolution ($\Delta\nu$ = 0.5, 1.0 cm^{-1}) makes it possible to increase the signal-to-noise ratio, a significant smoothing of the spectrum makes the "separation of the different variables problematical (i.e., the contributions of variations from different values of T_i).

5. We formulate the primary results and conclusions of this paper.

(1) The breakdown in LTE has a significant effect on the formation of the spectral structure

Table 2

Variations in the Outgoing Limb Radiance along Slant Paths (ν_0 = 617.8 cm^{-1}, $\Delta\nu$ = 0.1 cm^{-1}), Attributable to Variations Different T_i [$erg \cdot s^{-1} \cdot cm^{-2} \cdot (cm^{-1})^{-1} \cdot sr^{-1}$]

Individual variations	h_0, km						
	50	60	70	80	90	100	110
$\delta I_{\Delta\nu}[\delta T(z)]$	−0,39	0,074	0,067	0,017	10^{-3}	10^{-3}	10^{-5}
$\delta I_{\Delta\nu}[\delta T_1(z)]$	−1,83	−0,49	−0,33	−0,16	−0,009	10^{-4}	10^{-5}
$\delta I_{\Delta\nu}[\delta T_2(z)]$	6,60	1,57	0,67	0,34	0,077	0,006	10^{-3}
$\delta I_{\Delta\nu}[\delta T_3(z)]$	−0,34	−0,026	10^{-3}	10^{-5}	—	—	—
$\delta I_{\Delta\nu}[\delta T_5(z)]$	1,48	0,43	0,03	0,002	10^{-3}	10^{-4}	—
Sum variation	5,52	1,56	0,44	0,20	0,07	0,006	10^{-3}

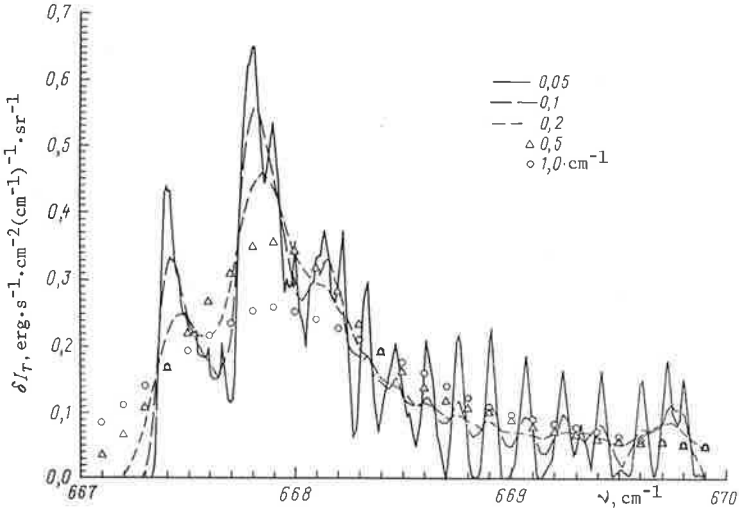

Fig. 6. Variations in the outgoing limb radiance attributable to temperature variations for a tangent height h_0 = = 90 km for different spectral resolutions cm^{-1}).

of the outgoing limb radiance on slant paths at the intensive lines of the 15 μm CO_2 band.

(2) The nonequilibrium effects are manifested in the final high resolution spectra for tangent altitudes substantially lower than the level of breakdown of LTE in the atmosphere.

(3) By using ultrahigh spectral resolution measurements, it is fundamentally possible to initiate sounding of a spherically inhomogeneous atmosphere.

(4) According to these estimates, the "optimal" spectral resolution for passive determination of the kinetic and vibrational temperatures in the 50 μm CO_2 band is $\Delta\nu \approx 0.2$ cm^{-1}, at which we have a maximum signal-to-noise ratio, and the spectral separation of variables attributable to different values of T_i is conserved.

(5) The absolute limb radiance variations attributable to variations in the kinetic temperature for the spectral regions and tangent heights analyzed here are not significant and demonstrate the difficulty of recovering information on vertical kinetic temperature profiles under conditions of a nonequilibrium atmosphere.

Received April 22, 1991;
revised October 24, 1991

REFERENCES

1. Kondrat'yev, K. Y. and Yu. M. Timofeyev. Meteorologicheskoye zondirovaniye atmosfery iz kosmosa (Space-Based Weather Atmospheric Sounding). Gidrometeoizdat Press, Leningrad, 1978.
2. Karol', I. L., V. V. Pozanov and Yu. M. Timofeyev. Gazovye primesi v atmosfere (Gas Impurities in the Atmosphere). Gidrometeoizdat Press, Leningrad, 1983.
3. Houghton, J. T., F. W. Taylor and C. D. Rodgers. Remote Sounding of Atmospheres. Cambridge University Press, Cambridge, 1984.
4. Kutepov, A. A. and Yu. M. Timofeyev. The effect of a breakdown of local thermodynamic equilibrium on the accuracy of thermal sounding of the upper atmospheric layers. Conference Proceedings of the Eleventh All-Union Conference on Actinometry. Talinin, pp. 105-108, 1980.
5. Dem'yanikov, A. I. and A. A. Kutepov. The possibility for remote thermal sounding of upper atmospheric layers on slant paths accounting for deviations from local thermodynamic equilibrium. Izv. AN SSSR. Fizika atmosfery i okeana, 23, No. 5, pp. 510-518, 1987.
6. Dem'yanikov, A. I. and A. A. Kutepov. The possibility for determining the radiation survival probability in the 15 μm CO_2 band based on remote sounding data. Izv. AN SSSR. Fizika atmosfery i okeana, 24, No. 4, pp. 387-393, 1988.
7. Zachor, A. S. and R. D. Sharma. Retrieval of non-LTE vertical structure from a spectrally resolved infrared limb radiance profile. J. Geophys. Res., 90, No. A1, pp. 467-475, 1985.
8. Carli, B. F. Mencaraglia and A. Bonetti. Submillimeter high-resolution FT spectrometer for atmospheric studies. Appl. Optics., 23, No. 15, pp. 2594-2603, 1984.
9. Michelson interferometer for passive atmospheric sounding on the European polar platform. Proposal to ESA, July, 1988.
10. Optical remote sensing of the atmosphere. 1990 Technical Digest Series, 4, p. 649, 1990.
11. Rothman, L. S. et al. The HITRAN database: 1986 edition. Appl. Optics, 26, No. 19, pp. 4058-4097, 1987.
12. Kutepov, A. A. and G. M. Shved. Transport of 15 μm CO_2 band radiation under non-LTE conditions in Earth's atmosphere. Izv. AN SSSR. Fizika atmosfery i oekana, 14, No. 1, pp. 28-43, 1978.
13. Anderson, G. P. et al. AFGL atmospheric constituent profiles (0-120 km). Envir. Res. Papers, No. 954, p. 44, 1986.
14. Timofeyev, Yu. M. and T. A. Dvorovik. Angular dependence of outgoing limb radiance in the 15 μm CO_2 band and restoration of a two-dimensional temperature profile. Materials of the Ninth All-Union Conference on Actinometry 10-13 October 1972. Gidrometoizdat Press, Leningrad, pp. 122-125, 1974.
15. Oelhaf, H. and H. Fischer. Relevance of upper atmosphere non-LTE effects to limb emission of stratospheric constituents. IRS'88: Current problems in atmospheric radiation. Ed. by J. Lenoble and J. F. A. Gellyn. Deepak Publishing Co., NY, pp. 460-463, 1989.